

# ProtoArgNet: Interpretable Image Classification with Super-Prototypes and Argumentation

Hamed Ayoobi  
Imperial College London  
United Kingdom  
h.ayoobi@imperial.ac.uk

Nico Potyka  
Cardiff University  
United Kingdom  
potykan@cardiff.ac.uk

Francesca Toni  
Imperial College London  
United Kingdom  
f.toni@imperial.ac.uk

## Abstract

We propose ProtoArgNet, a novel interpretable deep neural architecture for image classification in the spirit of prototypical-part-learning as found, e.g. in ProtoPNet. While earlier approaches associate every class with multiple prototypical-parts, ProtoArgNet uses super-prototypes that combine prototypical-parts into single prototypical class representations. Furthermore, while earlier approaches use interpretable classification layers, e.g. logistic regression in ProtoPNet, ProtoArgNet improves accuracy with multi-layer perceptrons while relying upon an interpretable reading thereof based on a form of argumentation. ProtoArgNet is customisable to user cognitive requirements by a process of sparsification of the multi-layer perceptron/argumentation component. Also, as opposed to other prototypical-part-learning approaches, ProtoArgNet can recognise spatial relations between different prototypical-parts that are from different regions in images, similar to how CNNs capture relations between patterns recognized in earlier layers.

## 1. Introduction

Deep neural architectures are successful in various tasks [22], including image classification (the focus of this paper). However, they tend to be mostly inscrutable black-boxes, whereas, especially in high-stakes settings, interpretability is crucial and interpretable models are advocated over black-boxes, especially if they achieve comparable performance [30].

Prototypical-part learning for image classification amounts to learning prototypical-parts of classes in images by introducing a *prototype layer* between a *convolutional backbone* and a *classifier* [6]. Prototypical-parts are latent representations of patches in images, like the beak or tail of a bird (see Figure 1 (a)). The prototype layer determines the similarity between prototypical-parts and patches in

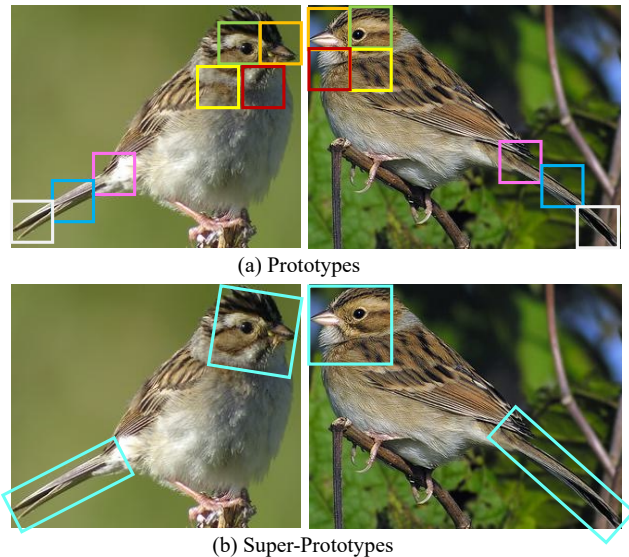


Figure 1. Conventional prototypes (a) versus the proposed super-prototypes (b) for a sample in the CUB-200-2011 dataset [38]. Super-prototypes can encode spatial correlation between prototypical-parts by combining low-level prototypes.

the latent space that the convolutional backbone maps to. Even though some prototypical-parts may correspond to background patches that are meaningless for humans (rather than exclusively meaningful parts in images as in Figure 1 (a)), they allow making transparent classifications, based on clearly defined prototypes, if the classifier is interpretable (e.g., logistic regression as in ProtoPNet [6]).

We propose *ProtoArgNet* (Section 4, overviewed in Figure 2), a novel interpretable deep neural architecture for image classification in the spirit of prototypical-part-learning. Similar to ProtoPShare [31] and ProtoTrees [26], ProtoArgNet shares prototypes among classes. However, while these and other prototypical-part-learning approaches associate every class with multiple prototypical parts, ProtoArgNet summarizes them in a single *super-prototypes* per

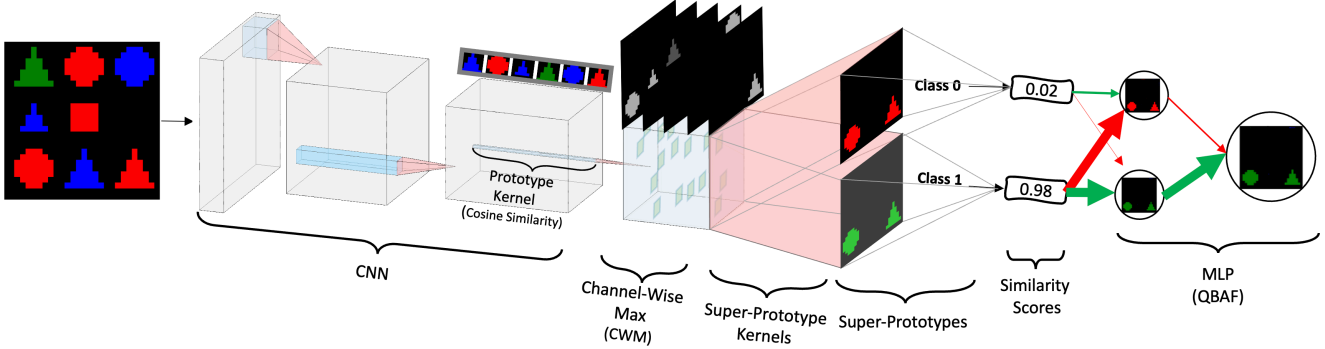


Figure 2. Architecture of ProtoArgNet (see Section 4 for the details), illustrated with a sample from the SHAPES dataset [17].

class that encodes spatial relationships between them (see Figure 1 (b) for an illustration).

The use of super-prototypes allows capturing spatial relationships between prototypical parts similar to how CNNs capture relations between patterns recognized in earlier layers. As we will demonstrate in the experiments with the SHAPES dataset [17], these relationships are essential for some classification tasks but state-of-the-art prototypical-part-learning approaches are unable to capture them. For example, in Figure 2, a positive example (Class 1) has a triangle in the left column and a circle in the right column on the same row. Merely recognizing prototypical-parts for triangles and circles in the input image (as in other prototypical-part-learning approaches) is insufficient for determining the class label in this example. ProtoArgNet effectively tackles this challenge by encoding the spatial relations between distinct prototypical-parts using the super-prototype kernels.

The classifier component in ProtoArgNet is a Multi-Layer Perceptron (MLP). ProtoArgNet addresses the lack of interpretability of (potentially deep) MLPs by integrating the SpArX methodology of [5] to translate the MLP to a sparse *quantitative bipolar argumentative framework* (QBAF) [28]. The QBAF explains the mechanics of the underlying MLP in terms of the roles played by the super-prototypes towards output classes, as well as hidden (clusters of) neurons. The ‘Arg’ in ProtoArgNet refers to this use of QBAFs, a well-known form of *argumentation* [3], where ‘arguments’ (amounting, in ProtoArgNet, to super-prototypes, clusters of neurons in the MLP, and predicted classes) can ‘attack’ or ‘support’ other ‘arguments’ (as indicated with red and green arrows in Figure 2)<sup>1</sup>, with a dialectical strength in line with activations in the MLP.

We show experimentally (Sections 5 and 6) that ProtoArgNet outperforms the state-of-the-art prototypical-part-learning models ProtoPNet [6], ProtoTree [26], ProtoP-

Share [31], ProtoPool [32] and PIP-Net [27] in terms of classification accuracy and the ability to encode and detect spatial relationships in images, supported by a number of ablations and the study of the cognitive complexity of local explanations derived from the sparsification of QBAFs obtained with ProtoArgNet.

## 2. Related Work

The problem of explaining the outputs of image classifiers is well studied in the literature, with approaches including, amongst others, feature attributions (e.g. as in [24, 29, 34]), attention maps (e.g. as in [33]), counterfactual explanations (e.g. as in [14]), and concept based methods (e.g. as in [12, 13]). These approaches fall under the category of *post-hoc explanations* for the outputs of models, specifically to be used when the models are black-boxes that need to be understood. We focus instead on developing an *interpretable* deep learning architecture based on prototypical-part-learning [35] and on argumentation [5]. We also illustrate how this model can naturally support argumentative forms of explainability [7]. In the remainder of this section we overview the most relevant literature to ProtoArgNet along three dimensions, as indicated.

**Prototypical-part-learning approaches** Prototypical-part-learning approaches were motivated by the observation that class-prototypes [23] for datasets with simple backgrounds (as in MNIST [10]) do not generalize well to natural images with more complex backgrounds. To overcome this problem, *ProtoPNet* [6] introduced prototypical parts for capturing parts of the class (like the beak or tail of a bird) rather than the whole object (the bird). The authors showed that it performs competitively on the more demanding CUB-200-2011 [38] and Cars [20] datasets. ProtoPNet learns prototypical parts as subpatches (with reduced height and width) of the output of a convolutional backbone. A prototype layer associates each class with  $m$  prototypes and determines the maximum similarity (inverse

<sup>1</sup>Please note that the colour of the shapes in the input image has no relation with or bearing on the colours of the super-prototypes and edges in the QBAF, indicating attack and support (see Section 4 for details).

Euclidean distance) between patches in the input image and prototypes. The classification is then made by logistic regression based on the individual similarity values.

*ProtoPShare* [31] improves ProtoPNet by sharing prototypes among classes. To this end, prototypes are pruned based on a data-dependent similarity between prototypes that measures the compliance on similarity scores for all patches in the training data. Similar prototypes are merged and can be shared between classes. Experiments (again with CUB-200-2011 and CARS) show that ProtoPShare can achieve the same performance as ProtoPNet while reducing the number of prototypes by 50-75%.

*ProtoTree* [26] builds on ProtoPNet by using a soft decision tree, rather than logistic regression, on top of the convolutional backbone. Every node in the tree learns a prototype similar to ProtoPNet’s prototype layer. While the trees grow exponentially in height, they can be pruned significantly and ProtoTree can achieve better performance than ProtoPNet (again on CUB-200-2011 and CARS) while reducing the number of prototypes by 90%.

It has been noted [16] that similarity in the latent space does not necessarily correspond to similarity in the image space and vice versa. This makes prototypical-part-learning approaches prone to adversarial manipulations resulting in explanations that are absurd for humans. *PIP-Net* [27] aims to address this issue by first creating pairs of images that share prototypes from single images by applying data augmentations and then adding an alignment term to the training objective that penalizes prototypes that are dissimilar for image pairs.

While these approaches need to integrate a step to prune a large number of trained prototypes, *ProtoPool* avoids this step using the Gumbel-Softmax trick [18], while reducing the required number of prototypes by sharing prototypes across all classes, similarly to ProtoPShare. Further, ProtoPool uses a focal similarity function to distinguish prototypes from less salient, background features.

ProtoArgNet differs from these state-of-the-art approaches in that it uses super-prototypes and MLPs/QBAFs, based on a novel architecture. We will use ProtoPNet, ProtoPShare, ProtoPool, ProtoTree and PIP-Net as baselines to evaluate ProtoArgNet’s performances.

**Argumentation** ProtoArgNet uses a form of argumentation (see [3] for a general overview of this research area), to maintain interpretability (lost with the use of MLPs rather than logistic regression or other interpretable methods in the state-of-the-art on prototypical-part-learning). Specifically, ProtoArgNet extends the *SpArX* approach [5], originally defined for MLPs with tabular data only, to the setting of prototypical-part-learning with images.

Several argumentation-based forms of explainability have been proposed, as overviewed e.g. in [7]. The use

of argumentation within ProtoArgNet paves the way to customizing ProtoArgNet to generate a variety of explanation formats. While doing so it is outside the scope of this paper it is an important avenue for future work.

Other works combine argumentation and image classification, e.g. [1, 37] for explaining the outputs of CNNs and [4] to obtain an interpretable image classifier. We focus on combining argumentation and the novel concept of super-prototypes for interpretability purposes.

**Neuro-symbolic approaches** ProtoArgNet may be deemed neuro-symbolic as it combines, end-to-end (see Figure 2), neural components (the convolutional backbone, the prototype kernels, and the super-prototype kernels) with symbolic argumentation frameworks (QBAFs) drawn from MLPs. However, whereas recent neuro-symbolic systems often combine purely symbolic with purely neural systems [8, 11, 25, 40], ProtoArgNet is based on the observation that MLPs can be seen as QBAFs and vice versa [5, 28]. Similar to neural architectures, the reasoning process in QAFs is associative rather than deductive. That is, arguments can positively or negatively influence the belief in other arguments via support or attack relationships. We keep the reasoning process in QBAFs interpretable by sparsification, as in [5]. Also, while many neuro-symbolic systems [2, 11, 25, 40], focus on integrating (symbolic) background knowledge into neural systems, ProtoArgNet is a neural system featuring a transparent reasoning process.

### 3. Preliminaries

We build up on SpArX [5], a post-hoc explanation method that aims at generating structurally faithful explanations for MLPs. SpArX exploits that MLPs can be understood as Quantitative Bipolar Argumentation Frameworks (QBAFs) [28]. QBAFs can be seen as graphical reasoning models whose nodes represent *arguments* and whose edges represent *attack* or *support* relations between the arguments, each with a (negative or positive, respectively) intensity value. Every argument in a QBAF is associated with an *initial strength* and reasoning algorithms determine a *final strength* (representing an acceptability degree) for every argument, based on its initial strength and the final strength of its attackers and supporters.

Arguments in QBAFs are abstract entities (what makes them arguments is that they are in dialectical relationships). To capture MLPs as in [28], these abstract arguments represent input features, hidden neurons and output classifications, and the graphical structure of QBAFs mirror the MLP. Roughly speaking, in order to transform an MLP into a QBAF, neurons can be associated with arguments, their biases can be transformed into initial strength values and their connection weights into intensity values of attack and

support relations. The translation guarantees that the activations of neurons in the original MLP correspond to the final strength values of arguments in the QBAF [28].

This correspondence allows representing MLPs faithfully by QBAFs, but the QBAF representation is not useful for interpretability and explainability, because the QBAF has the same size as the original MLP. Thus, SpArX clusters neurons with similar activations and summarizes each cluster as a single argument [5]. Naturally, a larger compression ratio (sparser graph) can result in larger unfaithfulness (average difference between the strength of the cluster argument and the activations of the neurons in the cluster). However, experiments with tabular data show that SpArX can give explanations that are both sparse and faithful [5].

In this work, we extend SpArX to make ProtoArgNet interpretable and explainable. An illustration is given in Figure 2: neurons in the MLP component of ProtoArgNet are treated as arguments, alongside the similarity scores from the super-prototypes, which serve as the input features for the MLP in our architecture (see the examples in Section 4 for further details on this illustration). Similarly to the original SpArX, we experiment with sparsification by various compression ratios (Section 6.5), showing that ProtoArgNet can provide explanations that are both sparse and faithful for image classification.

## 4. ProtoArgNet

Figure 2 shows the architecture of ProtoArgNet. ProtoArgNet consists of a convolutional backbone  $f$  with weights  $W^{conv}$ , a prototype layer  $\mathcal{P}$ , a Channel-Wise Max (CWM) layer  $\mathcal{CWM}$ , a Super-Prototype kernel  $\mathcal{SP}$  followed by an MLP  $\mathcal{MLP}$  with weights  $W^{\mathcal{MLP}}$ , mapped onto a QBAF for interpretability and explainability purposes. We discuss each component in turn, assuming that inputs are images and the classification task amounts to predicting a class in the set  $K$  ( $|K| \geq 2$ ).

### 4.1. Prototypes

Let  $z = f(x)$  be the convolutional output for an input image  $x$ , where the output tensor  $z$  has shape  $H \times W \times D$  with height  $H$ , width  $W$  and  $D$  channels. This output tensor serves as input to the prototype layer,  $\mathcal{P}$ , which represents prototypical-parts.  $\mathcal{P}$  consists of  $N$  prototypes  $P = \{p_i\}_{i=1}^N$  with shapes  $H_1 \times W_1 \times D$  (we have used  $H_1 = W_1 = 1$  in all experiments). For each prototype  $p_i \in P$  and every  $H_1 \times W_1 \times D$  sub-tensor  $z_j$  of  $z$ , the prototype layer  $\mathcal{P}$  computes the cosine similarity

$$\mathcal{CS}(p_i, z_j) = \frac{p_i \cdot z_j}{\|p_i\| \|z_j\|} \quad (1)$$

and outputs a similarity map

$$\mathcal{SM}_i = \mathcal{CS}_{z_j \in z}(p_i, z_j) \quad (2)$$

with shape  $H \times W$  for each prototype  $p_i \in P$ . Intuitively,  $\mathcal{SM}_i$  indicates how similar the prototypical-part  $p_i$  is to patches of the input image  $x$  in the latent space. We implemented  $\mathcal{SM}$  using the 2D convolution operator  $*$ . It generates  $\mathcal{SM}_i$  by convoluting the normalized convolutional output  $\hat{z} = \frac{z}{\|z\|} = \left[ \frac{z_j}{\|z_j\|} \right]_{z_j \in z}$  with a normalized prototype kernel  $\hat{p}_i = \frac{p_i}{\|p_i\|}$ ,  $\mathcal{SM}_i = \hat{z} * \hat{p}_i$ . Since cosine similarity is used for the prototype layer, the values in similarity maps can be both positive and negative in the range  $[-1, 1]$ . The output dimensions of the prototype layer are  $H \times W \times N$ .

### 4.2. Channel-Wise Max

The Channel-Wise Max layer aims to both localize and extract the max value of each similarity map while maintaining its dimensions.  $\mathcal{CWM}$  takes the similarity maps as input and extracts the maximum value from each input channel by passing the maximum value and setting all other values to zero while preserving the input dimensions. Formally, for every similarity value  $s \in \mathcal{SM}_i$ , the  $i^{\text{th}}$  similarity map, the channel-wise max filter  $\mathcal{CWM}_i$  retains the highest value  $s_{max} = \max(\mathcal{SM}_i)$  within the map and assigns a value of zero to the remaining elements:

$$\mathcal{CWM}_i = \begin{cases} s_{max} & \text{if } s = \max(\mathcal{SM}_i); \\ 0 & \text{otherwise.} \end{cases} \quad (3)$$

The output dimensions of  $\mathcal{CWM}$  are still  $H \times W \times N$ .

### 4.3. Super Prototypes and Similarity Scores

The super-prototypes kernel takes the output of the channel-wise max layer as input and provides a single similarity score per class. This is done in three steps.

In the first step, for each class  $k \in K$ ,  $M$  linear combinations of the channel-wise max filters, denoted by  $\mathcal{LC}_i^k$  where  $i \in \{1, \dots, M\}$ , are learned. Here,  $M$  is a customisable hyper-parameter of the model ( $M = 32$  achieved the best results in the experiments). Formally:

$$\mathcal{LC}_i^k = \sum_{j=1}^N w_j^{\mathcal{LC}_i^k} \cdot \mathcal{CWM}_j \quad (4)$$

where  $w_j^{\mathcal{LC}_i^k}$  is a trainable scalar weight. We let  $W^{\mathcal{LC}}$  denote the vector summarizing all these weights. This operation can be implemented with  $M$  convolutions with kernel shape  $1 \times 1 \times N$  using the  $N$  channel-wise max filters as input.

In the second step, the super-prototypes are constructed. Each linear combination  $\mathcal{LC}_i^k$  is then multiplied by a trainable weight matrix  $W_i^{\mathcal{SP}^k}$  with shape  $H \times W$  to obtain a single super-prototype for each class from the  $M$  linear combinations. This means that the number of super-prototypes



is equal to the number of classes  $|K|$ . Each super-prototype  $\mathcal{SP}^k$  is then computed as follows:

$$\mathcal{SP}^k = \sum_{i=1}^M \mathcal{LC}_i^k \odot W_i^{\mathcal{SP}^k}, \quad (5)$$

where  $\odot$  denotes element-wise product. Each super-prototype has the shape  $H \times W$ . By utilizing the receptive field of the convolutional output  $f$  to rescale the similarity maps  $\mathcal{SM}$  to the input dimensions, the super-prototypes can be visualized on the input image  $x$  employing Equation 5, as illustrated next.

**Example 1.** Figure 2 illustrates the visualization of the super-prototypes on the input image, where the colours indicate support (green) for Class 1 at the bottom and attack (red) against Class 0 at the top. Note that, since we are dealing with binary classification in this example, the supporting regions for accepting one class are the attacking regions for accepting the other class. Also, the colours in the input images are irrelevant to the classification task which associates Class 1 to images with a triangle in the left column and a circle in the right column on the same row, no matter their colour.

In the third and final step, a single similarity score  $ss_k$  is computed for each super-prototype by summing up the values  $sp \in \mathcal{SP}^k$ :

$$ss^k = \sum_{sp \in \mathcal{SP}^k} sp. \quad (6)$$

Equations 5 and 6 can be simultaneously implemented by employing  $|K|$  convolutions with a kernel shape of  $H \times W \times M$ , while taking the  $M$  linear combinations for each class as input.

#### 4.4. Classifier Layer

Using the similarity scores as input,  $\mathcal{MLP}$  is used for classification. After the training phase,  $\mathcal{MLP}$  is converted to a QBAF (c.f., Section 3 – this involves sparsifying the underlying  $\mathcal{MLP}$  and then translating it to a QBAF). The obtained QBAF can provide reasons for and against assigning an input  $x$  to a specific class, making ProtoArgNet interpretable as illustrated next.

**Example 2.** The (sparsified) 1-hidden layer-MLP/QBAF in Figure 2 can be interpreted as follows:

- the super-prototype for Class 1 supports and attacks, with high intensity, the arguments corresponding to, respectively, the bottom and top (clusters of) neurons in the hidden layer;
- conversely, the super-prototype for Class 0 attacks and supports, with low intensity, the same arguments;

- the hidden clusters and output neurons are visualized using the super-prototypes they “propagate” through the MLP, in the sense that these super-prototypes support them, e.g. the super-prototype for Class 0 supports the top cluster in the hidden layer and the predicted Class 1 is supported by the super-prototype for Class 1.

Overall, this interpretation indicates that the predicted Class 1 for the input image is supported by the presence of a circle in the bottom left corner and a triangle in the bottom right corner, while also pointing to the reasoning of the MLP in terms of the super-prototypes used.

## 5. Training ProtoArgNet

Unlike other prototypical-part-learning approaches, the training phase of ProtoArgNet is done in one step. This means that all amongst the prototype layer, the super-prototype kernels and the classifier are trained at once without a need for freezing the weight of the classifier first and fine-tuning it later. For the  $i^{\text{th}}$  data point in a dataset of size  $n$ , with the data point belonging to class label  $y_i \in K$  (where  $K$  is the set of class labels), the target class super-prototype should obtain a high similarity score  $ss_{y_i}$ . Moreover, the corresponding similarity scores for the super-prototypes of other classes ( $\{ss_k\}_{k=1, k \neq y_i}^{|K|}$ ) should be low. Simultaneously, the output of the classifier should be 1 for the target class  $y_i$  and 0 for the other classes. Therefore, we integrate in the loss function two components  $L_{\mathcal{SP}}$  and  $L_{cls}$  for the corresponding objectives.

**Definition 1.** The total loss function  $\mathcal{L}$  that we aim to minimize is:

$$\mathcal{L} = L_{CE} + L_{\mathcal{SP}} \quad (7)$$

where

- $L_{CE}$  is the Cross-Entropy loss :

$$L_{CE} = \sum_{i=1}^n \text{CrsEnt}(G(x_i), y_i), \quad (8)$$

where  $G(x_i)$  denotes the output of ProtoArgNet.

- $L_{\mathcal{SP}}$  is a regularization term that aims at associating super-prototypes with their associated classes by penalizing the similarity to wrong classes and rewarding the similarity to the correct class:

$$L_{\mathcal{SP}} = \sum_{i=1}^n \left( \left( \sum_{\substack{k=1 \\ k \neq y_i}}^{|K|} ss_k \right) - ss_{y_i} \right); \quad (9)$$

Given this definition of total loss function  $\mathcal{L}$ , we then use the Adam optimizer [19] to tune the convolutional weights

$W^{conv}$ , prototypes  $\mathcal{P}$ , linear combination weights  $W^{LC}$ , super-prototype weights  $W^{SP}$ , and MLP weights  $W^{MLP}$  simultaneously in an end-to-end fashion to minimize  $\mathcal{L}$ :

$$\min_{W^{conv}, \mathcal{P}, W^{LC}, W^{SP}} \mathcal{L}(W^{conv}, \mathcal{P}, W^{LC}, W^{SP}) \quad (10)$$

Finally, for the projection of prototypes, we follow the same approach as ProtoPNet [6] to push the prototypes to the latent representation of the closest image patch from the input space in the convolutional output so that each prototype has a global interpretable representation from the input space.

## 6. Experiments

We have compared our approach with the state-of-the-art prototypical-part-learning models ProtoPNet [6], ProtoTrees [26], ProtoPShare [31], ProtoPool [32] and PIP-Net [27]. We have conducted four sets of experiments to evaluate the classification performance (Section 6.2), the role of each layer on the model’s performance by an ablation study (Section 6.3), the ability to encode and detect spatial relationships in the input (Section 6.4), and the cognitive complexity of explanations naturally drawn from ProtoArgNet (Section 6.5). Notice that, for all the experiments, we use top-1 accuracy (which is just standard accuracy) as our measure of performance, as is the case with the baselines.

For all the experiments, we have used CUB-200-2011 [38] and Stanford CARS [20], which are the standard benchmarks for prototypical-part learning models.<sup>2</sup> To show that ProtoArgNet can identify spatial relationships that other methods fail to detect, we also use (an adaptation to binary classification of) the SHAPES dataset [17].

### 6.1. Experimental Setup

For all the experiments, the input images are resized to  $224 \times 224$ . We have set the number of prototypes  $N$  to 1024, and the number of linear combinations  $M$  to 32.<sup>3</sup> For training the model, we have set the batch-size to 32 and the number of epochs to 1000. Moreover, we have set the convolutional backbone to ResNet-50 [15] pre-trained using ImageNet [9]. The choices of batch-size, number of training epochs, and convolutional backbone and the pre-trained weights are aligned with previous prototypical-part-learning approaches. Finally, we used a one-layer MLP classifier with 100 hidden neurons with ReLU activation functions<sup>4</sup>.

<sup>2</sup>For the ablation study, we include additional experiments with small-scale datasets (MNIST [10], Fashion MNIST [39], CIFAR10 [21] and GT-SRB [36]) in the supplementary material section C.

<sup>3</sup>The performance of ProtoArgNet with various choices for  $N$  (512, 1024, 2048) and  $M$  (16, 32, 64, 128), is reported in the supplementary material section A.

<sup>4</sup>The performance of ProtoArgNet employing various MLP configurations, encompassing 1 to 5 hidden layers and a range of hidden neurons (50, 100, 200, and 400), is detailed in the supplementary material section B.

Method	Accuracy		
	CUB	CARS	SHAPES
ProtoPNet	79.2 ± 0.1	86.1 ± 0.1	51.1 ± 0.7
ProtoPShare	74.7 ± 0.2	86.4 ± 0.2	50.4 ± 0.8
ProtoPool	80.3 ± 0.2	88.9 ± 0.1	50.8 ± 0.6
ProtoTrees	82.2 ± 0.7	86.6 ± 0.2	51.4 ± 0.7
PIP-Net	82.0 ± 0.3	86.5 ± 0.3	50.6 ± 0.6
ProtoArgNet	<b>83.4 ± 0.2</b>	<b>89.3 ± 0.2</b>	<b>98.4 ± 0.2</b>

Table 1. Accuracy of ProtoArgNet and other prototypical-part-learning methods on the CUB-200-2011, Stanford Cars and SHAPES datasets. SHAPES is used for the evaluation of spatial correlation between prototypical-parts. (Best accuracy in **bold**)

Super-Prototypes	Prototype Layer	Classifier	Accuracy	
			CUB	CARS
—	L2	Fixed	79.2	86.1
—	L2	MLP	81.2	86.7
—	Cosine	Fixed	81.5	87.2
—	Cosine	MLP	81.8	87.8
✓	L2	Fixed	81.0	87.3
✓	L2	MLP	81.6	87.9
✓	Cosine	Fixed	82.7	88.9
✓	Cosine	MLP	<b>83.4</b>	<b>89.3</b>

Table 2. Ablation study with different prototype layers and classifiers with respect to a super-prototype kernel. (Best accuracy in **bold**)

### 6.2. Classification Performance

The first two columns in Table 1 show the accuracy of our method compared to the baselines, for CUB-200-2011 and Stanford CARS. For both datasets, our ProtoArgNet outperforms the other approaches.

### 6.3. Ablation study

Ablation studies on CUB-200-2011 and CARS in Table 2 show that ProtoArgNet achieves the best accuracy when employing super-prototypes atop the cosine similarity prototype layer, together with an MLP as classifier component. Alternatively, the L2-distance-based prototype layer, as utilized in ProtoPNet, can be employed in conjunction with a fixed logistic regression layer for classification (fine-tuned in the second training phase in ProtoPNet). Notably, ProtoArgNet surpasses the performance of state-of-the-art methods even when utilizing a fixed logistic regression layer, instead of an MLP as the classifier (but performs best with the MLP).

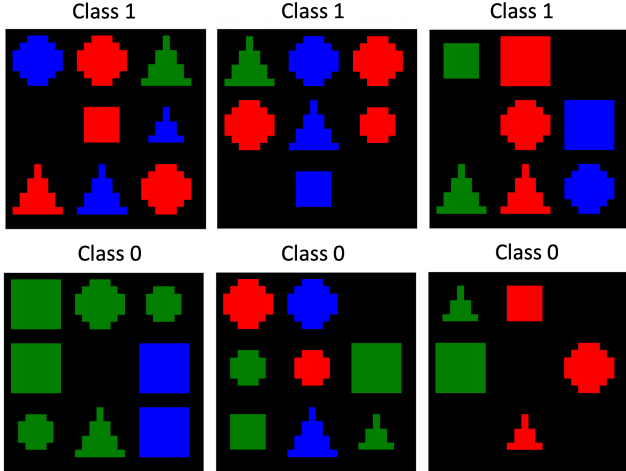


Figure 3. Example images from (our adaptation of) the SHAPES dataset, with binary class labels. The first row contains images from class 1, where a triangle is located in the first column and a circle is located in the third column of the same row. The second row contains images from class 0, where this condition is not met.

#### 6.4. Spatial Correlations

To assess whether different image classification methods can account for spatial relationships between prototypical-parts in images, we adapted the SHAPES dataset [17] as a benchmark. We randomly generated synthetic images containing  $3 \times 3$  grids of circles, triangles, and squares in different colours (red, green, and blue), so that an image is assigned Class 1 if a triangle is located in the first column and a circle is located in the third column of the same row<sup>5</sup>, and Class 0 otherwise. The resulting dataset comprises 10,000  $28 \times 28$  images with balanced binary class labels. Figure 3 shows examples of images in the dataset.

The last column in Table 1 compares the accuracy of the baselines for this SHAPES dataset. ProtoArgNet, with an accuracy of  $98.4\% \pm 0.2\%$ , significantly outperforms all other approaches. The accuracy of the other approaches is around 50%, suggesting that these models are unable to infer class labels solely based on the presence of prototypes in images, being unable to infer information about the relative placement of the prototypical-parts in the images. ProtoArgNet addresses this limitation by using channel-wise max and super-prototypes, which enable the model to infer the spatial correlation of different prototypical-parts in the image when needed for classification.

#### 6.5. Cognitive Complexity of Explanations

The combination of super-prototypes and QBAFs can serve as the basis for human-readable local explanations for the

<sup>5</sup>This criterion can be customized to reflect the user’s preferences. For example, the dataset could assign Class 1 to images with a square in the first column, a blue triangle in the second, and a red square in the third.

outputs of ProtoArgNet. Figure 2 showed a generated local explanation for a data point in SHAPES (see the examples in Section 4 for details on this illustration). Figure 4 illustrates a local explanation generated for a data instance from the CUB-200-2011 dataset, specifically for the target class “Baird Sparrow.” The green overlay on the super-prototype highlights the region in the input image that supports the classification of the instance as a “Baird Sparrow,” while the red region identifies the attacked or unsupported portion of the input. This super-prototype can be interpreted as the bird’s head resembles a “Baird Sparrow,” but its tail is atypical for this species. We have added this reading manually here for illustration, simulating how a human may read the super-prototypes. We leave the automatic generation of human-readable interpretations of the super-prototypes and the QBAF for explanatory purposes to future work.

We can use the number of representative (super-)prototypes as a measure of the cognitive complexity of the explanations drawn from prototypical-part-learning methods. Table 3 compares the number of (super-)prototypes for each approach, before and after the pruning phase if applicable. Since ProtoPool and ProtoTrees use an ensemble of multiple models, we have also reported the corresponding number of prototypes for these cases. Like ProtoPool, our ProtoArgNet does not have a pruning phase for pruning unnecessary prototypes. The number of super-prototypes in our approach is equal to the number of classes since ProtoArgNet has one super-prototype per class. Notice that using a fixed classification layer, as in ProtoPNet, for ProtoArgNet, the local explanations require only one super-prototype while other approaches need multiple prototypes.

The global cognitive complexity of ProtoArgNet should additionally include the number of hidden nodes in the MLP since each node in the resulting QBAF would be part of the explanation. This complexity can be controlled by sparsification as in SpArX [5], with a trade-off between compression ratio of the MLP classifier and accuracy of the resulting ProtoArgNet model. For illustration, considering a one-layer MLP and 10 arguments in the QBAF after the sparsification of the MLP, the cognitive complexity of the QBAF would be 210 and 206 for the CUB-200-2011 and the Stanford Cars dataset, respectively.

We have experimented with various degrees of sparsification, where the sparser (more compressed) the QBAF the more cognitively manageable the explanations but the higher the possibility of unfaithfulness (drop of accuracy) with respect to the original MLP. Table 4 shows the effect of compression ratio on the accuracy of a one-layer MLP with 100 hidden neurons. These results indicate that even with a high compression ratio of 0.8 for the MLP, the model can still maintain a high accuracy (and thus faithfulness).

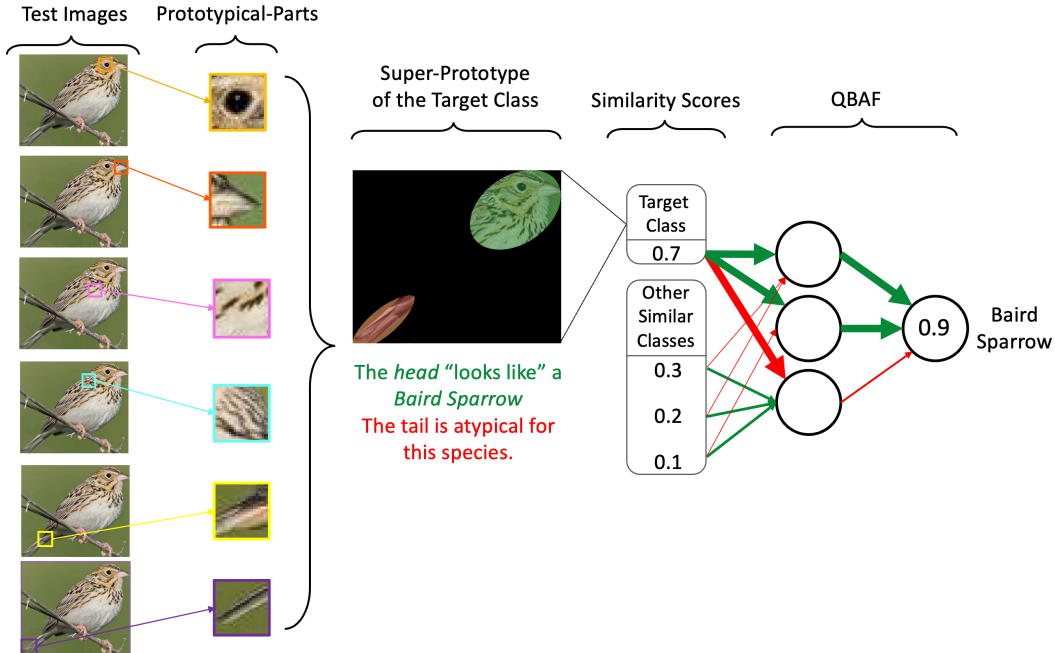


Figure 4. An example of ProtoArgNet explanation for an image belonging to the *Baird Sparrow* target class from the CUB-200-2011 dataset. The prototypical-parts are learned from the image patches in the training set. The super-prototype highlights the supported regions with a green overlay and the attacked / unsupported regions with a red overlay. The output neuron in the MLP/QBAF assigns the probability of 0.9 for classifying the input image as a *Baird Sparrow*. The QBAF outlines the reasoning of the MLP.

	Method	# Prototypes / # Super-Prototypes	
		CUB	CARS
Before Pruning	ProtoPNet	2000	2000
	ProtoPShare	2000	2000
	ProtoPool	202 / 202×5	<b>195</b> / 195×5
	ProtoTrees	512	512
	PIP-Net	2000	2000
	ProtoArgNet	<b>200</b>	196
After Pruning	ProtoPNet	2000	1960
	ProtoPShare	400	480
	ProtoPool	—	—
	ProtoTrees	202 / 202×3	<b>195</b> / 195×3
	PIP-Net	495	515
	ProtoArgNet	—	—

Table 3. Comparison of the number of prototypes/super-prototypes for different approaches before and after pruning step. For ProtoPool and ProtoTrees, we also report the ensemble cases.

## 7. Conclusion

We proposed ProtoArgNet, a novel prototypical-part-learning approach. ProtoArgNet learns a single super-prototype per class. The super-prototypes integrate multiple prototypical-parts shared between different classes into

Compression Ratio	Accuracy	
	CUB	CARS
0.2	83.1 ± 0.2	89.2 ± 0.2
0.4	82.9 ± 0.1	88.9 ± 0.1
0.6	82.5 ± 0.2	88.4 ± 0.1
0.8	81.8 ± 0.2	88.1 ± 0.2

Table 4. Accuracy of ProtoArgNet with different compression ratios of the MLP for the CUB-200-2011 and Stanford Cars datasets.

a representative prototype per class. It can be trained end-to-end and does not require an additional pruning phase. As opposed to previous prototypical-part-learning approaches, the use of super-prototypes allows ProtoArgNet to capture spatial relationships between prototypical-parts. Using an MLP for classification allows ProtoArgNet to capture non-linear relationships between super-prototypes, while applying the SpArX methodology allows explaining the classification outcome. Experiments show that ProtoArgNet outperforms state-of-the-art prototypical-part-learning approaches in terms of accuracy and the ability to model spatial relationships between prototypical-parts.

Future directions include expanding ProtoArgNet’s capabilities to encompass multi-modal data. Additionally, we will investigate the implementation of a user-model feed-



back loop to enhance the debugging process for super-prototypes. Further, we plan to deploy ProtoArgNet with real data, e.g. in the medical domain. Finally, we plan to explore various options for obtaining explanations from ProtoArgNet, including interactive forms thereof [7].

## **8. Acknowledgments**

This research was partially funded by the European Research Council (ERC) under the European Union's Horizon 2020 research and innovation programme (grant agreement No. 101020934, ADIX) and by J.P. Morgan and by the Royal Academy of Engineering under the Research Chairs and Senior Research Fellowships scheme. Any views or opinions expressed herein are solely those of the authors.

# ProtoArgNet: Interpretable Image Classification with Super-Prototypes and Argumentation

## Supplementary Material

### A. (Super-)Prototypes Configurations

The performance of ProtoArgNet with various choices for the number of prototypes  $N$  (512, 1024, 2048) and the number of linear combinations  $M$  (16, 32, 64, 128) is reported in Table 5. The results show that  $M = 32$  and  $N = 1024$  is the best choice for both CUB-200-2011 and Stanford cars datasets.

$N$	$M$	Datasets	
		CUB	CARS
512	16	82.5	87.6
512	32	82.9	88.1
512	64	82.6	87.7
512	128	82.2	87.1
1024	16	83.0	88.2
1024	32	<b>83.4</b>	<b>89.3</b>
1024	64	82.8	88.4
1024	128	82.3	87.6
2048	16	82.5	88.2
2048	32	82.9	88.6
2048	64	82.5	88.1
2048	128	82.1	87.8

Table 5. The accuracy of ProtoArgNet with different numbers of prototypes  $N$  and linear combinations  $M$ . (Best accuracy in **bold**)

### B. MLP/QBAF Configurations

Table 6 shows the performance of ProtoArgNet employing various MLP configurations, encompassing 1 to 5 hidden layers and a range of hidden neurons (50, 100, 200, and 400). The results show that an MLP with 1 hidden layer and 100 neurons achieves the best accuracy.

### C. Additional Ablation Studies

We have conducted further ablation studies with popular small-scale datasets, including MNIST [10], Fashion MNIST [39], CIFAR10 [21] and GTSRB [36] as shown in Table 7. The results suggest that cosine similarity outperforms L2-distance and MLP is a better classifier than a logistic regression with initial fixed weights for the first phase of training. Moreover, the super-prototypes layer boosts the accuracy of the model in all cases. This confirms the results in the main body of the paper.

# Hidden Layers	# Hidden Neurons	Datasets	
		CUB	CARS
1	50	82.3	88.7
1	100	<b>83.4</b>	<b>89.3</b>
1	200	83.2	88.9
1	400	82.4	88.3
2	50	81.7	88.4
2	100	82.3	88.6
2	200	81.5	88.3
2	400	81.1	87.8
3	50	80.8	88.3
3	100	80.4	88.5
3	200	80.1	88.1
3	400	79.9	87.6
4	50	80.3	88.0
4	100	79.5	88.3
4	200	79.3	87.7
4	400	79.2	87.4
5	50	80.2	87.8
5	100	79.3	88.0
5	200	78.5	87.3
5	400	78.1	86.9

Table 6. ProtoArgNet accuracy with different MLP/QBAF configurations. (Best accuracy in **bold**)

### References

- [1] Emanuele Albini, Piyawat Lertvittayakumjorn, Antonio Rago, and Francesca Toni. DAX: deep argumentative explanation for neural networks. *CoRR*, abs/2012.05766, 2020. 3
- [2] Yaniv Aspis, Krysia Broda, Jorge Lobo, and Alessandra Russo. Embed2sym - scalable neuro-symbolic reasoning via clustered embeddings. In *International Conference on Principles of Knowledge Representation and Reasoning, (KR 2022)*, 2022. 3
- [3] Katie Atkinson, Pietro Baroni, Massimiliano Giacomin, Anthony Hunter, Henry Prakken, Chris Reed, Guillermo Ricardo Simari, Matthias Thimm, and Serena Villata. Towards artificial argumentation. *AI Mag.*, 38(3):25–36, 2017. 2, 3
- [4] H. Ayoobi, M. Cao, R. Verbrugge, and B. Verheij. Argue to learn: Accelerated argumentation-based learning. In *20th IEEE International Conference on Machine Learning and Applications (ICMLA)*, 2021. 3
- [5] Hamed Ayoobi, Nico Potyka, and Francesca Toni. SpArX: Sparse argumentative explanations for neural networks.

Super-Prototype	Prototype	Classifier	Datasets			
			MNIST	Fashion	CIFAR10	GTSRB
—	L2	Fixed	96.35	86.31	83.42	98.14
—	L2	MLP	97.26	87.41	83.94	98.37
—	Cosine	Fixed	97.91	88.16	84.13	98.73
—	Cosine	MLP	98.21	88.71	84.49	99.33
✓	L2	Fixed	97.35	87.94	83.96	98.86
✓	L2	MLP	97.72	88.31	84.21	99.29
✓	Cosine	Fixed	98.47	89.68	84.83	99.44
✓	Cosine	MLP	<b>99.15</b>	<b>90.41</b>	<b>85.24</b>	<b>99.89</b>

Table 7. Ablation study with different prototype and classifier layers with respect to a super-prototype layer for additional small-scale datasets. (Best accuracy in **bold**)

- In *European Conference on Artificial Intelligence (ECAI)*, pages 149–156. IOS Press, 2023. [2](#), [3](#), [4](#), [7](#)
- [6] Chaofan Chen, Oscar Li, Daniel Tao, Alina Barnett, Cynthia Rudin, and Jonathan K Su. This looks like that: deep learning for interpretable image recognition. *Advances in neural information processing systems*, 32, 2019. [1](#), [2](#), [6](#)
- [7] Kristijonas Cyras, Antonio Rago, Emanuele Albin, Pietro Baroni, and Francesca Toni. Argumentative XAI: A survey. In *Proceedings of the Thirtieth International Joint Conference on Artificial Intelligence, IJCAI 2021*, 2021. [2](#), [3](#), [9](#)
- [8] Alessandro Daniele, Tommaso Campari, Sagar Malhotra, and Luciano Serafini. Deep symbolic learning: Discovering symbols and rules from perceptions. In *Proceedings of the Thirty-Second International Joint Conference on Artificial Intelligence, IJCAI 2023, 19th-25th August 2023, Macao, SAR, China*, 2023. [3](#)
- [9] Jia Deng, Wei Dong, Richard Socher, Li-Jia Li, Kai Li, and Li Fei-Fei. ImageNet: A large-scale hierarchical image database. In *2009 IEEE Conference on Computer Vision and Pattern Recognition*, pages 248–255, 2009. [6](#)
- [10] Li Deng. The MNIST database of handwritten digit images for machine learning research. *IEEE Signal Processing Magazine*, 29(6):141–142, 2012. [2](#), [6](#), [1](#)
- [11] Ivan Donadello, Luciano Serafini, and Artur S. d’Avila Garcez. Logic tensor networks for semantic image interpretation. In *International Joint Conference on Artificial Intelligence (IJCAI 2017)*, pages 1596–1602. ijcai.org, 2017. [3](#)
- [12] Asma Ghandeharioun, Been Kim, Chun-Liang Li, Brendan Jou, Brian Eoff, and Rosalind W Picard. DISSECT: Disentangled simultaneous explanations via concept traversals. *arXiv:2105.15164*, 2021. [2](#)
- [13] Amirata Ghorbani, James Wexler, James Zou, and Been Kim. Towards automatic concept-based explanations. *arXiv:1902.03129*, 2019. [2](#)
- [14] Yash Goyal, Ziyang Wu, Jan Ernst, Dhruv Batra, Devi Parikh, and Stefan Lee. Counterfactual visual explanations. In *ICML*. PMLR, 2019. [2](#)
- [15] Kai Ming He, Xiangyu Zhang, Shaoqing Ren, and Jian Sun. Deep residual learning for image recognition. In *2016 IEEE Conference on Computer Vision and Pattern Recognition (CVPR)*, pages 770–778, 2016. [6](#)
- [16] Adrian Hoffmann, Claudio Fanconi, Rahul Rade, and Jonas Kohler. This looks like that... does it? shortcomings of latent space prototype interpretability in deep networks. *arXiv preprint arXiv:2105.02968*, 2021. [3](#)
- [17] Ronghang Hu, Jacob Andreas, Marcus Rohrbach, Trevor Darrell, and Kate Saenko. Learning to reason: End-to-end module networks for visual question answering. In *2017 IEEE International Conference on Computer Vision (ICCV)*, pages 804–813, 2017. [2](#), [6](#), [7](#)
- [18] Eric Jang, Shixiang Gu, and Ben Poole. Categorical reparameterization with gumbel-softmax. In *5th International Conference on Learning Representations, ICLR 2017, Toulon, France, April 24-26, 2017, Conference Track Proceedings*. OpenReview.net, 2017. [3](#)
- [19] Diederik P. Kingma and Jimmy Ba. Adam: A method for stochastic optimization. In *3rd International Conference on Learning Representations, ICLR 2015, San Diego, CA, USA, May 7-9, 2015, Conference Track Proceedings*, 2015. [5](#)
- [20] Jonathan Krause, Michael Stark, Jia Deng, and Li Fei-Fei. 3d object representations for fine-grained categorization. In *2013 IEEE International Conference on Computer Vision Workshops*, pages 554–561, 2013. [2](#), [6](#)
- [21] Alex Krizhevsky. Learning multiple layers of features from tiny images. 2009. [6](#), [1](#)
- [22] Yann LeCun, Yoshua Bengio, and Geoffrey Hinton. Deep learning. *nature*, 521(7553):436–444, 2015. [1](#)
- [23] Oscar Li, Hao Liu, Chaofan Chen, and Cynthia Rudin. Deep learning for case-based reasoning through prototypes: A neural network that explains its predictions. In *Proceedings of the AAAI Conference on Artificial Intelligence*, 2018. [2](#)
- [24] Scott M Lundberg and Su-In Lee. A unified approach to interpreting model predictions. In *NeurIPS*, 2017. [2](#)
- [25] Robin Manhaeve, Sebastijan Dumancic, Angelika Kimmig, Thomas Demeester, and Luc De Raedt. DeepProbLog: Neural probabilistic logic programming. In *Advances in Neural Information Processing Systems (NeurIPS 2018)*, pages 3753–3763, 2018. [3](#)
- [26] Meike Nauta, Ron van Bree, and Christin Seifert. Neural prototype trees for interpretable fine-grained image recognition. In *IEEE Conference on Computer Vision and Pattern*

- Recognition (CVPR 2021)*, pages 14933–14943. Computer Vision Foundation / IEEE, 2021. [1](#), [2](#), [3](#), [6](#)
- [27] Meike Nauta, Jörg Schlötterer, Maurice van Keulen, and Christin Seifert. Pip-net: Patch-based intuitive prototypes for interpretable image classification. In *Proceedings of the IEEE/CVF Conference on Computer Vision and Pattern Recognition (CVPR 2023)*. Computer Vision Foundation / IEEE, 2023. [2](#), [3](#), [6](#)
- [28] Nico Potyka. Interpreting neural networks as quantitative argumentation frameworks. In *Proceedings of the Thirty-Third AAAI Conference on Artificial Intelligence, (AAAI-21)*, 2021. [2](#), [3](#), [4](#)
- [29] Marco Tulio Ribeiro, Sameer Singh, and Carlos Guestrin. ” why should i trust you?” explaining the predictions of any classifier. In *Proceedings of the 22nd ACM SIGKDD international conference on knowledge discovery and data mining*, pages 1135–1144, 2016. [2](#)
- [30] Cynthia Rudin. Stop explaining black box machine learning models for high stakes decisions and use interpretable models instead. *Nat. Mach. Intell.*, 1(5):206–215, 2019. [1](#)
- [31] Dawid Rymarczyk, Lukasz Struski, Jacek Tabor, and Bartosz Zielinski. ProtoPSHare: Prototypical parts sharing for similarity discovery in interpretable image classification. In *SIGKDD Conference on Knowledge Discovery and Data Mining (KDD)*, pages 1420–1430. ACM, 2021. [1](#), [2](#), [3](#), [6](#)
- [32] Dawid Rymarczyk, Łukasz Struski, Michał Górszczak, Koryna Lewandowska, Jacek Tabor, and Bartosz Zieliński. Interpretable image classification with differentiable prototypes assignment. In *Computer Vision – ECCV 2022: 17th European Conference, Tel Aviv, Israel, October 23–27, 2022, Proceedings, Part XII*, page 351–368, Berlin, Heidelberg, 2022. Springer-Verlag. [2](#), [6](#)
- [33] Sam Sattarzadeh, Mahesh Sudhakar, Konstantinos N Plataniotis, et al. Integrated grad-cam: Sensitivity-aware visual explanation of deep convolutional networks via integrated gradient-based scoring. In *IEEE Int. Conf. on Acoustics, Speech and Signal Processing (ICASSP)*, 2021. [2](#)
- [34] Avanti Shrikumar, Peyton Greenside, and Anshul Kundaje. Learning important features through propagating activation differences. In *ICML*, 2017. [2](#)
- [35] Jake Snell, Kevin Swersky, and Richard Zemel. Prototypical networks for few-shot learning. *Advances in neural information processing systems*, 30, 2017. [2](#)
- [36] J. Stallkamp, M. Schlipsing, J. Salmen, and C. Igel. Man vs. computer: Benchmarking machine learning algorithms for traffic sign recognition. *Neural Networks*, 32:323–332, 2012. Selected Papers from IJCNN 2011. [6](#), [1](#)
- [37] Purin Sukpanichnant, Antonio Rago, Piyawat Lertvitayakumjorn, and Francesca Toni. Neural QBAFs: Explaining neural networks under lrp-based argumentation frameworks. In *AIxIA 2021 - Advances in Artificial Intelligence - 20th International Conference of the Italian Association for Artificial Intelligence, Virtual Event, December 1-3, 2021, Revised Selected Papers*, pages 429–444. Springer, 2021. [3](#)
- [38] C. Wah, S. Branson, P. Welinder, P. Perona, and S. Belongie. Caltech-UCSD Birds-200-2011 (CUB-200-2011). Technical Report CNS-TR-2011-001, California Institute of Technology, 2011. [1](#), [2](#), [6](#)
- [39] Han Xiao, Kashif Rasul, and Roland Vollgraf. Fashion-MNIST: a novel image dataset for benchmarking machine learning algorithms. *ArXiv*, abs/1708.07747, 2017. [6](#), [1](#)
- [40] Zhun Yang, Adam Ishay, and Joohyung Lee. Neurasp: Embracing neural networks into answer set programming. In *International Joint Conference on Artificial Intelligence, (IJCAI 2020)*, pages 1755–1762. ijcai.org, 2020. [3](#)